scientific reports

Check for updates

OPEN

Palladium nanoparticles immobilized on DT-CH-modified $MgFe_2O_4$@APTES magnetic nanoparticles as an efficient and reusable new catalyst for C-C coupling reactions

Magda Abdel lattif H[1]✉, Mohammad Abu Shuheil[2]✉, Munthar Abosaoda[3,4], M. M. Rekha[5], Rasha Eldalawy[6], Subhashree Ray[7], Kattela Chennakesavulu[8] & Renu Sharma[9]

A novel protocol has been developed for synthesizing a DT-CH-Pd complex anchored on $MgFe_2O_4$ nanoparticles, referred to as $MgFe_2O_4$@APTES@DT-CH-Pd. The structure of this nanomagnetic catalyst was thoroughly analyzed using various techniques, including FT-IR, XRD, FE-SEM, EDX, ICP, TGA, VSM, and N_2 adsorption-desorption isotherm analysis. Subsequently, its catalytic performance was evaluated in Suzuki cross-coupling reactions conducted in water, highlighting its use as a green solvent. Palladium loading on the catalyst was quantified through ICP analysis, measuring at 1.7×10^{-3} mol g^{-1}. This methodology offers several advantages, such as straightforward preparation from readily available materials, excellent catalytic activity, ease of operation, short reaction times, high yields, and an environmentally friendly solvent system. Importantly, the nanocatalyst was conveniently recovered using an external magnet and reused multiple times without notable degradation in catalytic efficiency.

Keywords Magnetic nanocomposite, $MgFe_2O_4$, Suzuki reaction, DTPA, Coupling reaction

Nanomaterials have gained substantial interest over the past decade owing to their unique chemical and catalytic characteristics[1–4]. One key area of application is their use as a substrate for immobilizing homogeneous catalysts, combining the benefits of both homogeneous and heterogeneous systems[5,6]. Within this realm, spinel metal oxides like ferrites have been extensively investigated in materials science and engineering due to their remarkable magnetic, electrical, and catalytic traits[7,8]. An exceptional example from the ferrite family is magnesium ferrite ($MgFe_2O_4$), which stands out for its robust magnetic properties and inverse spinel structure[9,10]. In this configuration, magnesium ions predominantly occupy octahedral sites, while iron ions are distributed across both tetrahedral and octahedral sites[11,12]. The unique architecture of $MgFe_2O_4$ allows it to fuse the advantageous magnetic features of both manganese and iron ferrites, making it highly versatile for applications such as data storage, magnetic hyperthermia therapy, catalysis, sensors, and electromagnetic wave absorption[13]. Heterogeneous magnetic catalysts represent a promising category within catalysis due to

[1]Centre for Research Impact & Outcome, Chitkara University Institute of Engineering and Technology, Chitkara University, Rajpura 140401, Punjab, India. [2]Department of Medical Laboratory Sciences, Faculty of Allied Medical Sciences, Hourani Center for Applied Scientific Research, Al-Ahliyya Amman University, Amman, Jordan. [3]College of Pharmacy, The Islamic University, Najaf, Iraq. [4]College of Pharmacy, The Islamic University of Al Diwaniyah, Al Diwaniyah, Iraq. [5]Department of Chemistry and Biochemistry, School of Sciences, JAIN (Deemed to be University), Bangalore, Karnataka, India. [6]College of Pharmacy, Al-Turath University, Al Mansour, Baghdad 10013, Iraq. [7]Department of Biochemistry, IMS and SUM Hospital, Siksha 'O' Anusandhan (Deemed to be University), Bhubaneswar 751003, Odisha, India. [8]Department of Chemistry, Sathyabama Institute of Science and Technology, Chennai, Tamil Nadu, India. [9]Department of Chemistry, University Institute of Sciences, Chandigarh University, Mohali, Punjab, India. ✉email: magda.lattif@atomicmail.io; abushuheilmohammad@gmail.com

their distinctive combination of magnetic characteristics and catalytic efficacy[14,15]. These materials present significant advantages, including simplified catalyst recovery, enhanced recyclability, and improved reaction kinetics[16,17]. Compared to conventional catalytic systems, heterogeneous magnetic catalysts streamline the recovery process, cut costs, and reduce environmental footprints[18,19]. Their ability to be recycled reinforces their potential for long-term sustainability and economic practicality, positioning them as an appealing choice for a wide array of catalytic applications[20,21]. Furthermore, the active sites located on the surface of the magnetic core or functionalized coatings support a diverse range of catalytic reactions, broadening their applicability across multiple domains[11,16,18,22]. The Suzuki reaction has become a cornerstone in various scientific domains, particularly due to its versatility in forming carbon-carbon bonds[23–25]. This reaction is extensively utilized in pharmaceutical synthesis, agricultural chemistry, polymer production, advanced material development, and natural product chemistry[26,27]. Its ability to efficiently create bonds between diverse components makes it an indispensable tool in constructing intricate molecules[28,29]. In pharmaceuticals, the Suzuki reaction plays a crucial role in the creation of drug molecules and intermediates[30]. Many significant pharmaceutical compounds feature complex carbon-carbon bond frameworks, which can be assembled with relative ease using this method. Beyond pharmaceuticals, the reaction's significance extends to materials science, where it aids in the development of conducting polymers, organic light-emitting diodes (OLEDs), organic solar cells, and nanoscale materials[31,32]. By enabling the polymerization of aryl and vinyl monomers often challenging to synthesize through other methods it facilitates precise control over polymer attributes such as chain length, molecular weight distribution, and overall structural design[33–35]. Its impact on organic chemistry is equally remarkable[36,37]. The synthesis of complex natural compounds, characterized by multi-ring structures and chiral centers, represents one of the field's most demanding challenges[38–40]. The Suzuki reaction provides a streamlined approach by enabling the integration of large and intricate building blocks into these molecules, thereby enhancing synthetic efficiency while shortening reaction pathways[5,41]. Notably, this methodology has been instrumental in producing biologically active natural products like alkaloids, terpenes, and steroids, which hold immense significance in medical and industrial applications[42,43].

The report details the development of an efficient heterogeneous catalyst, DT-CH-Pd, supported on $MgFe_2O_4$ magnetic nanoparticles and tailored for C-C coupling reactions. The findings demonstrate that the catalyst exhibits performance comparable to its homogeneous counterpart. Moreover, it provides the added benefit of easy recovery from the reaction mixture while maintaining nearly full catalytic activity.

Experimental

Preparation of $MgFe_2O_4$@APTES@DT-CH-Pd

The synthesis process for $MgFe_2O_4$ nanoparticles (NPs) began with the preparation of 3 mmol of $Mg(NO_3)_2{\cdot}6H_2O$ and 6 mmol of $FeCl_3{\cdot}6H_2O$. These components were combined and stirred in a water bath maintained at 80 °C for 30 min. Following this, 4 g of NaOH was introduced into the mixture, which was stirred continuously for 24 h. The resulting particles were separated using a straightforward magnetic method, thoroughly washed multiple times with water, and subsequently dried at 60 °C, as outlined in Fig. 1. To functionalize the material, 3.5 mL of 3-aminopropyltrimethoxysilane (APTES) was carefully introduced into a suspension containing 1 g of $MgFe_2O_4$ dispersed in 50 mL of toluene. This mixture was stirred under a nitrogen atmosphere at reflux conditions for 24 h to ensure thorough reaction. After the silanization process, the solid product was magnetically separated and dried at ambient temperature for 24 h before further modification. Subsequently, 1 g of nano-$MgFe_2O_4$@APTES was dispersed in a 1:1 ethanol-acetic acid solution (v/v) using an ultrasonic bath for 15 min. Afterwards, 2.5 mmol of diethylenetriaminepentaacetic acid (DTPA) was added to this dispersion, and the mixture was stirred at reflux for another 24 h. The resulting $MgFe_2O_4$@APTES@DT nanoparticles were recovered magnetically and sequentially washed with ethanol/acetic acid (1:1, v/v), water, and methanol. These multi-carboxyl-modified magnetic silica gels were then oven-dried at 60 °C for 12 h. For further functionalization, 1 g of $MgFe_2O_4$@APTES@DT was added to 30 mL of DMF and subjected to sonication for 15 min. Following this, 2 g of DCC was introduced, and 0.8 g of chitosan dissolved in a 25 mL solution of acetic acid (2.0% v/v) was gradually added to the system at room temperature. Upon complete chemical addition, the mixture was heated to 60 °C and maintained for 24 h. The resulting microgel was cooled to room temperature and thoroughly washed with deionized water. Next, 1 g of $MgFe_2O_4$@APTES@DT-CH was dispersed in ethanol, and 2.5 mmol of palladium acetate ($Pd(OAc)_2$) was added. This mixture underwent reflux for 24 h, after which 0.5 g of sodium borohydride ($NaBH_4$) was incorporated and allowed to react for an additional 3 h. The final nanoparticles, $MgFe_2O_4$@APTES@DT-CH-Pd, were isolated via magnetic decantation, rinsed with ethanol, and air-dried for further use as outlined in Fig. 1.

Preparation of Suzuki reaction

Phenylboronic acid (1 mmol), an aryl halide (1 mmol), and K_2CO_3 (1.1 mmol) were added to 3 mL of water in the presence of $MgFe_2O_4$@APTES@DT-CH-Pd magnetic nanoparticles (0.02 g). The reaction mixture was stirred under reflux, with its progress monitored by thin-layer chromatography (TLC). Upon completion, the mixture was allowed to cool, and the magnetic nanoparticles were separated using an external magnet. These were then washed thoroughly with water and ethyl acetate. The remaining solution was subjected to liquid–liquid extraction using water and ethyl acetate. The organic phase was dried using 0.9 g of anhydrous sodium sulfate (K_2SO_4). After evaporating the ethyl acetate, pure biphenyl derivatives were obtained in excellent yields, as shown in Fig. 2.

Selected NMR data

1,1'-biphenyl:^{1}H NMR (400 MHz, DMSO) (Figure.S$_1$): $\delta_H = 7.5$ (m, 10 H), ppm.

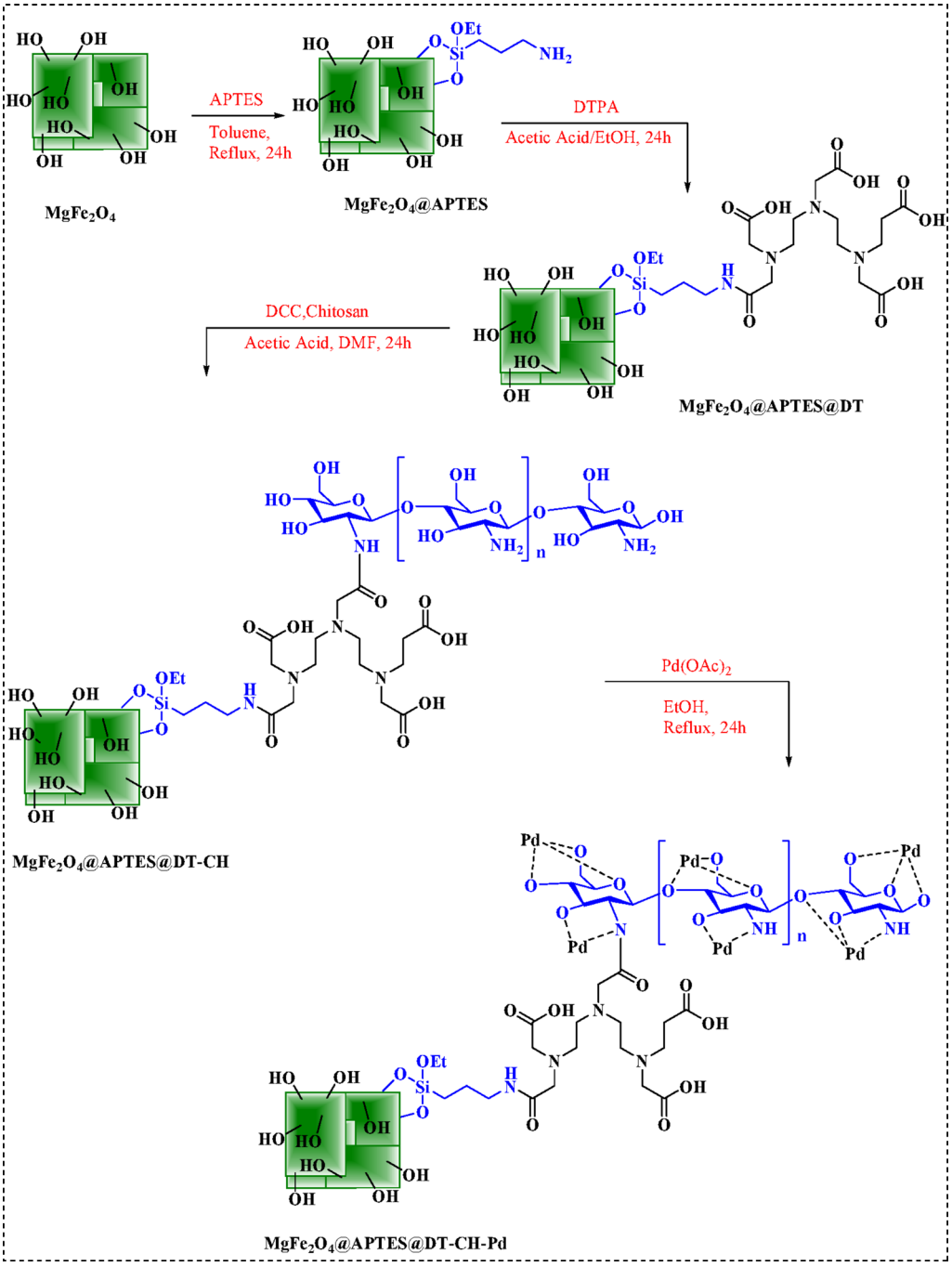

Fig. 1. Synthesis of $MgFe_2O_4$@APTES@DT-CH-Pd.

3-nitro-1,1'-biphenyl:^{1}H NMR (400 MHz, DMSO) (Figure.S_2): $\delta_H = 8.2$ (d, 2 H), 7.5 (m, 7 H), ppm.
1,1':4',1"-terphenyl:^{1}H NMR (400 MHz, DMSO) (Figure.S_3): $\delta_H = 7.6$ (s, 4 H), 7.3 (s, 4 H), 7.0 (m, 6 H), ppm.
4-methyl-1,1'-biphenyl:^{1}H NMR (400 MHz, DMSO) (Figure.S_4): $\delta_H = 7.8$ (s, 1H), 6.6 (m, 2 H), 7.4 (d, 6 H), 1.0 (s, 3 H) ppm.

Catalyst characterizations

To investigate the surface properties of composite nanoparticles, their molecular structure was analyzed using FT-IR spectra (Fig. 3). The characteristic absorption peak at 592 cm^{-1} for $MgFe_2O_4$ corresponds to the Fe–O bond's stretching vibration. This peak was consistently observed across all spectra, confirming the presence of $MgFe_2O_4$ nanoparticles in the intermediates and final products (Fig. 3a). Following functionalization with APTMS, new absorption peaks at 2985 and 2919 cm^{-1} emerged, representing the symmetric vibrations of aliphatic C–H stretching within the methylene group of the silane coupling agent. This indicates successful grafting of amino groups onto the $MgFe_2O_4$ surface (Fig. 3b). Subsequent grafting of multi-carboxyl groups

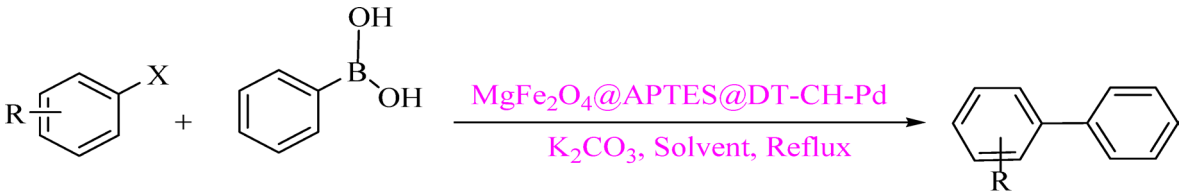

X= I, Cl, Br

R= NO_2, Me, OMe, OH, Ar, Cl, CHO, CN

Fig. 2. $MgFe_2O_4$@APTES@DT-CH-Pd catalyzed Suzuki coupling reactions.

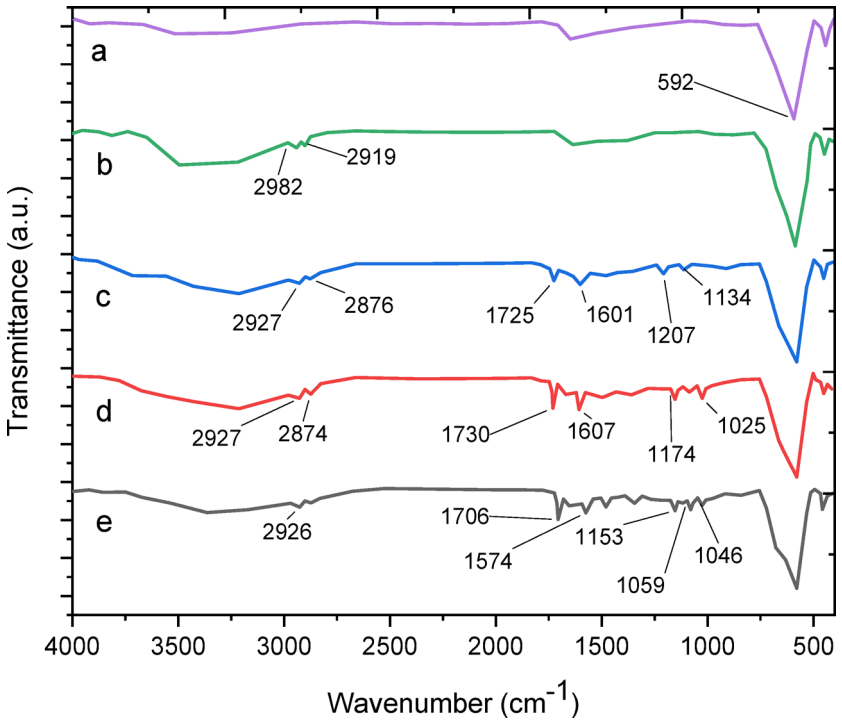

Fig. 3. Comparative study of FTIR spectra of (a) $MgFe_2O_4$, (b) $MgFe_2O_4$@APTES, (c) $MgFe_2O_4$@APTES@DT, (d) $MgFe_2O_4$@APTES@DT-CH, (e) $MgFe_2O_4$@APTES@DT-CH-Pd.

introduced strong absorption bands at 1725 and 1207 cm^{-1}, attributed to the C=O and C–O stretching vibrations of the –COO– group, confirming the formation of carboxylic groups (DT) on the nanoparticle surface (Fig. 3c). Chitosan was then grafted onto the magnesium ferrite surface. While the N–H stretching band at 3400 cm^{-1} overlapped with hydroxy group bands, the N–H bending mode at 1025 cm^{-1}, along with evidence of C–O–C groups, confirmed the presence of chitosan. Additionally, C–H stretching vibrations at 2927 and 2874 cm^{-1} indicated aliphatic CH groups in chitosan (Fig. 3d). Finally, due to significant palladium content on the nanoparticle surface, reductions in C=O and C–O vibrations suggest that the carboxyl groups on the magnetic silica surface functionally coordinate palladium, verifying the successful immobilization of palladium complexes on the $MgFe_2O_4$@APTES@DT-CH surface (Fig. 3e.)[44–48].

The X-ray diffraction (XRD) analysis of the $MgFe_2O_4$@APTES@DT-CH-Pd nanocomposite, as shown in Fig. 4, reveals distinct diffraction peaks at 2θ angles of 30°, 35°, 43°, 53°, 57°, and 63°. These peaks are associated with the (220), (311), (400), (422), (511), and (440) crystal planes, indicative of the cubic spinel structure characteristic of MgFe2O4. This confirms the successful synthesis of $MgFe_2O_4$ nanoparticles. Importantly, the crystal structure of $MgFe_2O_4$ remained preserved even after surface modification with various organic functional groups. Additionally, using the Debye–Scherrer formula, the mean crystal size of $MgFe_2O_4$@APTES@DT-CH-Pd MNPs was calculated to be 16.69 nm[49,50].

The thermal behavior of the $MgFe_2O_4$@APTES@DT-CH-Pd nanocomposite was evaluated using thermogravimetric analysis (TGA), as depicted in Fig. 5. The analysis identified two distinct stages of weight loss. The first stage, occurring below 250 °C, was linked to the evaporation of the adsorbed solvent. The second stage, noted between 250 and 700 °C, revealed a prominent weight loss of approximately 15%, which was attributed

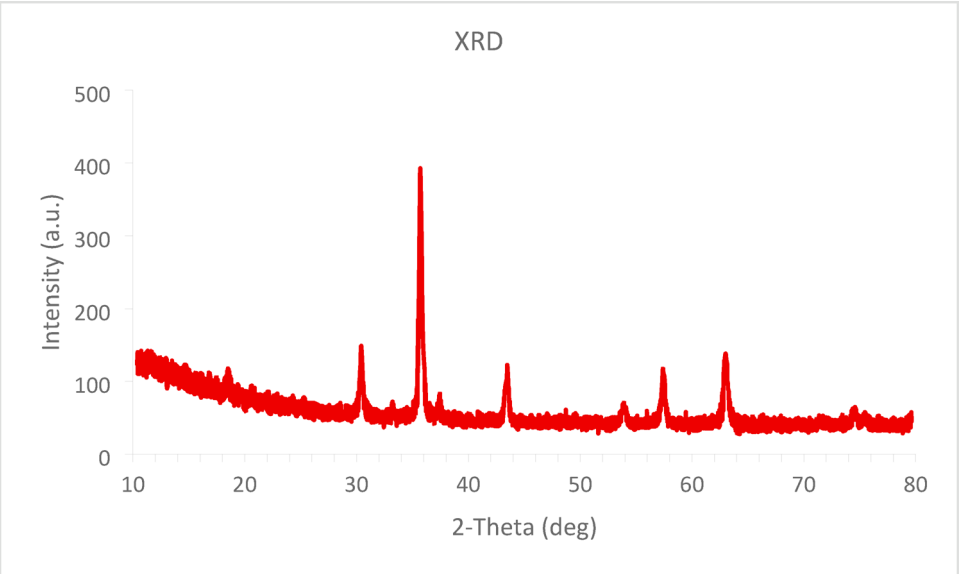

Fig. 4. XRD spectrum of $MgFe_2O_4$@APTES@DT-CH-Pd.

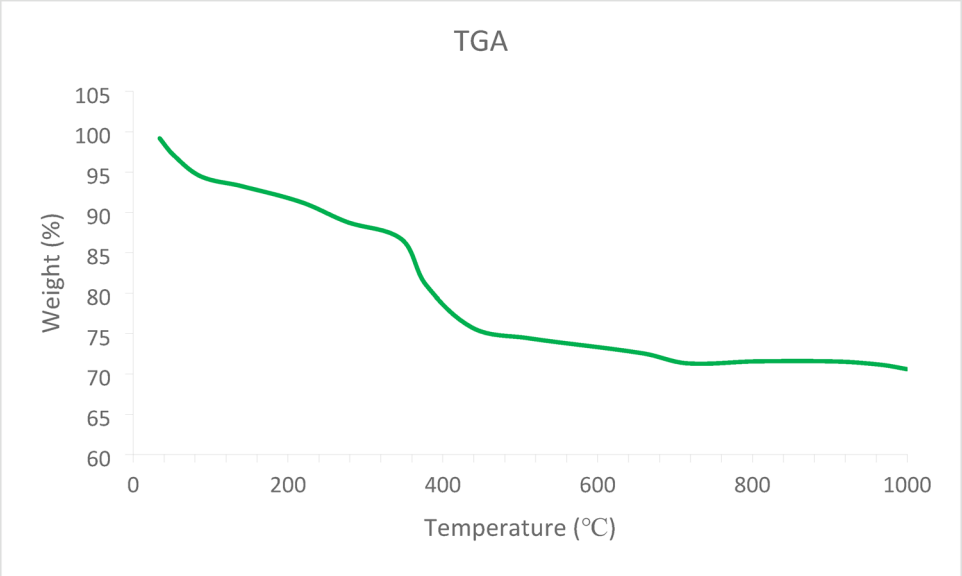

Fig. 5. TGA curve of $MgFe_2O_4$@APTES@DT-CH-Pd.

to the thermal decomposition of the organic layer and the palladium (Pd) complex bonded to it. These results emphasize the existence of a strong chemical bond between the DT-CH-Pd complex and the surface of the $MgFe_2O_4$ magnetic nanoparticles.

The elemental composition of $MgFe_2O_4$@APTES@DT-CH-Pd was assessed using an EDX spectrum, as depicted in Fig. 6. This analysis confirmed the presence of nitrogen, oxygen, iron, carbon, magnesium, silicon, and palladium within the catalyst, demonstrating the successful synthesis of the nanoparticles. Furthermore, it verified the effective immobilization of DT-CH-Pd onto the surface of the $MgFe_2O_4$ magnetic nanoparticles. To measure the palladium content in $MgFe_2O_4$@APTES/CC/GA-Pd, ICP-OES analysis indicated a Pd concentration of 1.7×10^{-3} mol g^{-1}. In addition, ICP analysis was conducted to evaluate palladium leaching after the catalyst was recycled. The results showed a Pd concentration of 1.6×10^{-3} mol g^{-1} in the reused catalysts, suggesting minimal Pd leaching from the $MgFe_2O_4$@APTES@DT-CH-Pd structure.

Scanning electron microscopy (SEM) was employed to assess and precisely characterize the size and structural attributes of the $MgFe_2O_4$@APTES@DT-CH-Pd nanocomposite. The resulting images, displayed in Fig. 7, reveal spherical particles with nanoscale dimensions, verifying the successful synthesis of nanoparticles with meticulous dimensional control.

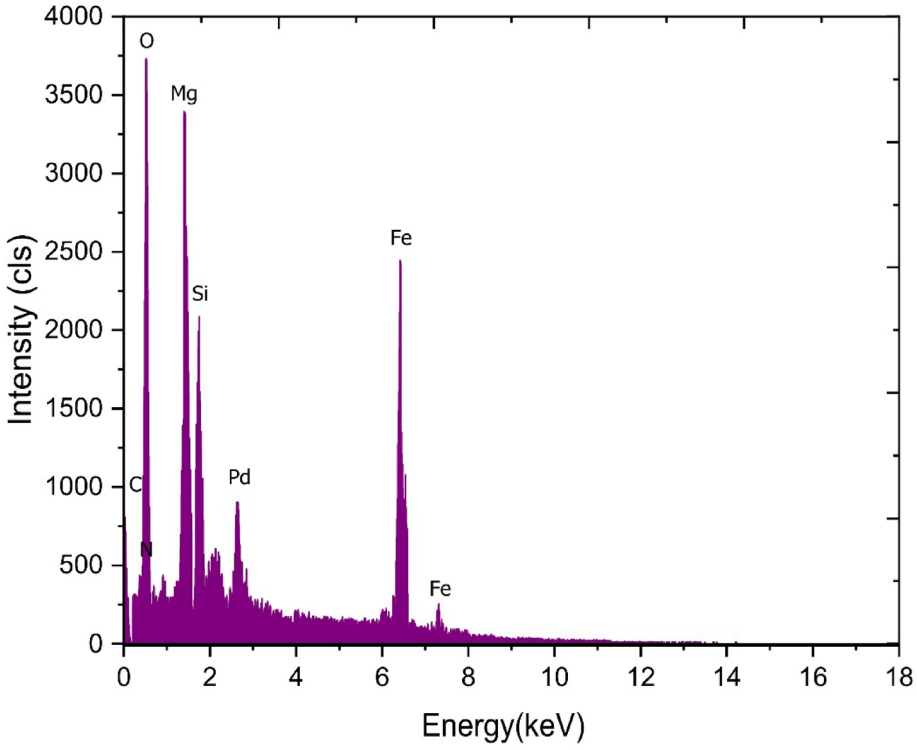

Fig. 6. EDS analysis of $MgFe_2O_4$@APTES@DT-CH-Pd.

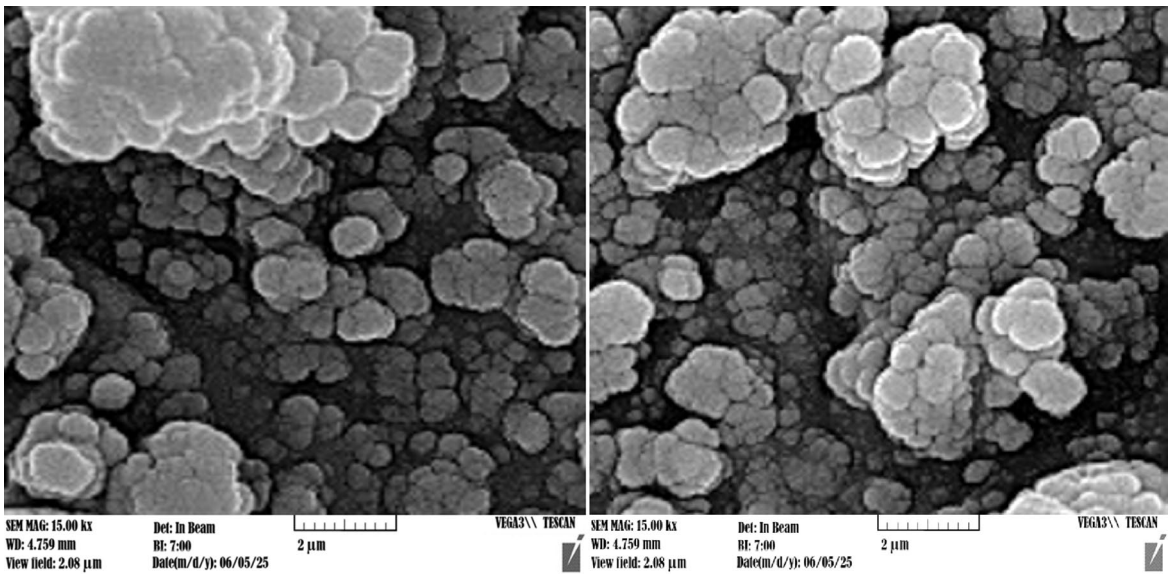

Fig. 7. SEM images of $MgFe_2O_4$@APTES@DT-CH-Pd.

The $MgFe_2O_4$@APTES@DT-CH-Pd complex was investigated using BET analysis to assess its isotherm type, surface area, and pore features, as depicted in Fig. 8. The analysis yielded values of 28.4 nm for average pore diameter, 41.36 m^2/g for specific surface area, and 0.062 cm^3/g for total pore volume. The nanocomposite demonstrated a type IV isotherm and revealed a mesoporous structure, as indicated by its pore characteristics. These surface attributes of the $MgFe_2O_4$@APTES@DT-CH-Pd complex offer abundant active sites for direct interactions with organic reactants, contributing to enhanced catalytic performance.

To assess the magnetic properties, uncoated magnetic spinel ferrite ($MgFe_2O_4$) and the $MgFe_2O_4$@APTES@DT-CH-Pd nanocomposite (MNPs) were analyzed using a vibrating sample magnetometer (VSM) at room temperature under an external magnetic field range of ± 10,000 Oe, as depicted in Fig. 9. The VSM analysis

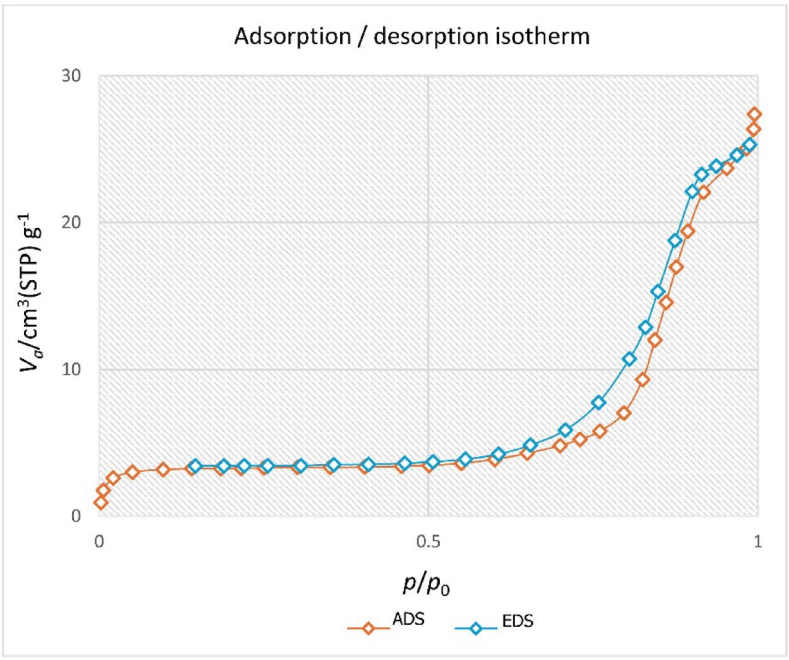

Fig. 8. The N_2 adsorption–desorption isotherm of $MgFe_2O_4$@APTES@DT-CH-Pd complex.

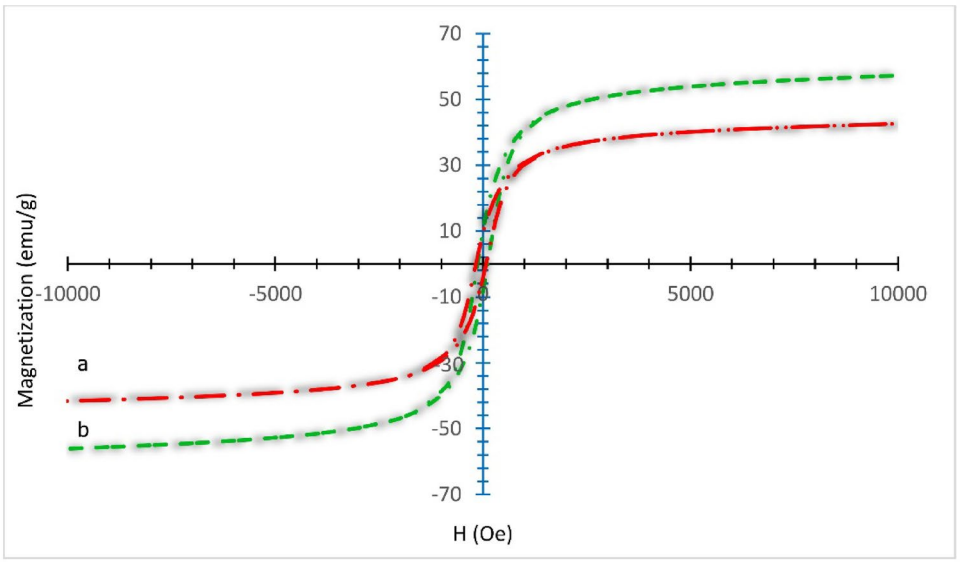

Fig. 9. VSM curves of (a) $MgFe_2O_4$ (b) $MgFe_2O_4$@APTES@DT-CH-Pd.

revealed a reduction in saturation magnetization (Ms), from approximately 53 emu/g for $MgFe_2O_4$ to around 32 emu/g for $MgFe_2O_4$@APTES@DT-CH-Pd. This decline in Ms is attributed to the presence of the newly applied coating layer, confirming the successful synthesis of the modified catalyst. Despite this lower magnetization, the $MgFe_2O_4$@APTES@DT-CH-Pd exhibits sufficient magnetic susceptibility to enable efficient magnetic separation across various reaction environments.

Catalytic studies

Following the successful synthesis and characterization of $MgFe_2O_4$@APTES@DT-CH-Pd magnetic nanoparticles, their catalytic efficiency in the Suzuki reaction was assessed. A model reaction was conducted, coupling iodobenzene (1 mmol) with phenylboronic acid (1 mmol), to identify the ideal reaction parameters. Various factors such as catalyst quantity, solvent choice, type of base, and reaction temperature were systematically examined, with the results summarized in Table 1. Initially, the impact of catalyst concentration was investigated, revealing that the highest yield was achieved using 0.02 g of $MgFe_2O_4$@APTES@DT-CH-Pd

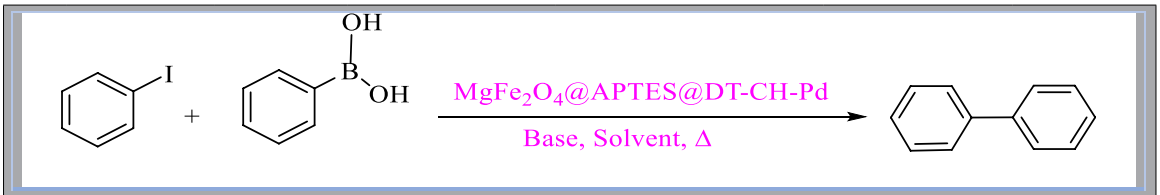

Entry	Cat. (g)	Solvent	Base	Temperature (°C)	Time (min)	Yield (%)
1	-	water	K_2CO_3	Reflux	24 h	-
2	0.008	water	K_2CO_3	Reflux	30	45
3	0.01	water	K_2CO_3	Reflux	30	60
4	0.02	water	K_2CO_3	Reflux	30	98
5	0.03	water	K_2CO_3	Reflux	30	98
6	0.02	PEG-400	K_2CO_3	120	30	54
7	0.02	Solvent Free	K_2CO_3	90	30	62
8	0.02	DMSO	K_2CO_3	100	30	75
9	0.02	EtOH	K_2CO_3	Reflux	30	70
10	0.02	DMF	K_2CO_3	100	30	63
11	0.02	water	KOH	Reflux	30	49
12	0.02	water	NaOH	Reflux	30	56
13	0.02	water	t-BuOK	Reflux	30	88
14	0.02	water	Na_2CO_3	Reflux	30	43
15	0.02	water	Et_3N	Reflux	30	39

Table 1. Optimizing the reaction between Phenylboronic acid and Iodobenzene using $MgFe_2O_4$@APTES@DT-CH-Pd as the catalytic system.

nanoparticles; notably, no reaction occurred in the absence of a catalyst. Further tests identified water as the optimal solvent and K_2CO_3 as the most effective base for the carbon-carbon coupling product under reflux conditions. Ultimately, the optimal parameters determined were 0.02 g of catalyst, 1.2 mmol of K_2CO_3, and water under reflux conditions.

Following optimization of the reaction conditions, the $MgFe_2O_4$@APTES@DT-CH-Pd (MNPs) magnetic nanoparticle catalyst was tested in Suzuki C-C cross-coupling reactions across a diverse range of aryl halides and phenylboronic acid. The catalyst demonstrated moderate to excellent efficiency in yielding biphenyl derivatives, effectively accommodating various aryl halides such as iodides, bromides, and chlorides with both electron-donating and electron-withdrawing substituents. Reactions involving aryl halides with electron-donating groups required longer times, likely due to their reduced activation during the oxidative addition step compared to electron-withdrawing substituents. The electrophilic reactivity pattern adhered to the order I > Br > Cl, with chlorides showing the least reactivity. However, the presence of DT-CH as a ligand alongside K_2CO_3 as a base enabled successful coupling of chlorides. In experiments utilizing 1-bromo-4-chlorobenzene, the bromide group exhibited higher reactivity than the chloride group, presenting a significant advantage for further functionalization of the resulting products (Table 2).

The catalytic cyclic mechanism of the Suzuki reaction employing the $MgFe_2O_4$@APTES@DT-CH-Pd catalyst follows three essential steps: oxidative addition, transmetalation, and reductive elimination. The process begins with the aryl halide interacting with the catalyst complex through oxidative addition, resulting in the formation of intermediate (1) This step is considered the most challenging phase of the cycle, where electron-donating oxygen groups present in the DT-CH ligand facilitate the cleavage of the Ar-X bond, effectively activating the Pd catalyst. Subsequently, intermediate 1 undergoes a transmetalation reaction involving the organoborane reagent and base, leading to the creation of intermediate (2) In the final stage, reductive elimination occurs, yielding the desired product while regenerating the $MgFe_2O_4$@APTES@DT-CH-Pd catalyst, which is then ready to participate in further catalytic cycles (Fig. 10).

Catalyst leaching study

The stability and heterogeneity of the $MgFe_2O_4$@APTES@DT-CH-Pd catalyst in the Suzuki reaction, specifically the coupling of iodobenzene and phenylboronic acid, were evaluated through a hot filtration experiment conducted midway through the reaction. During the initial test, the product yield at this stage reached 55%. In a subsequent experiment where the catalyst was removed at the same point, the reaction proceeded slightly further, resulting in a small increase in yield to 57%, after which no additional progress was noted. These observations suggest that at least palladium is leaching from the catalyst during the reaction.

Catalyst recyclability

Recovering and reusing nanocatalysts represent a critical feature in catalytic processes. To evaluate this functionality, we studied the performance of the recycled catalyst in the model reaction under optimized conditions. The findings revealed that the reused catalyst retained consistent efficiency, successfully enabling

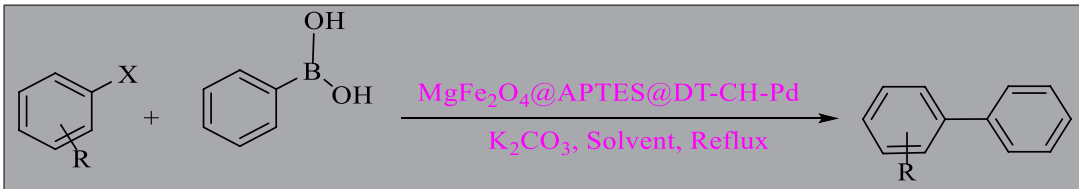

X= I, Cl, Br

R= NO_2, Me, OMe, OH, Ar, Cl, CHO, CN

Entry	Aryl halide	Product	Time (min)	Yield (%)	TON	TOF (min^{-1})
1	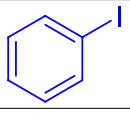	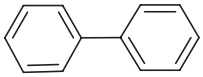	30	98	28.8	57.6
2	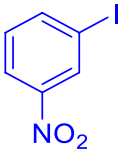	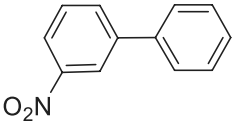	60	92	27.0	27.0
3	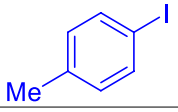	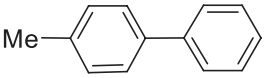	30	94	27.6	55.2
4	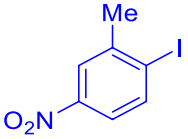	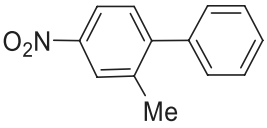	45	95	27.9	37.2
5	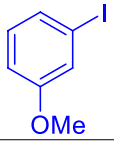	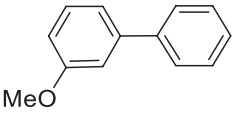	30	93	27.3	54.6
6	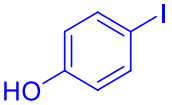	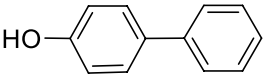	30	96	28.2	56.4
7	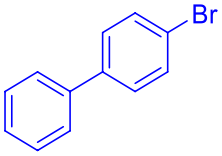	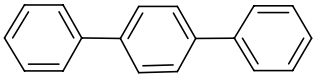	120	81	23.8	11.9
8	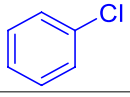	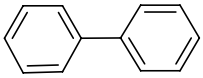	60	90	26.4	26.4
9	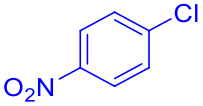	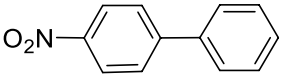	60	90	26.4	26.4
10	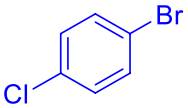	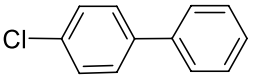	45	92	27.0	36
11	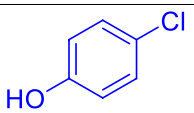	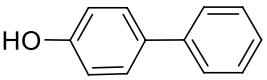	30	94	27.6	55.2

Continued

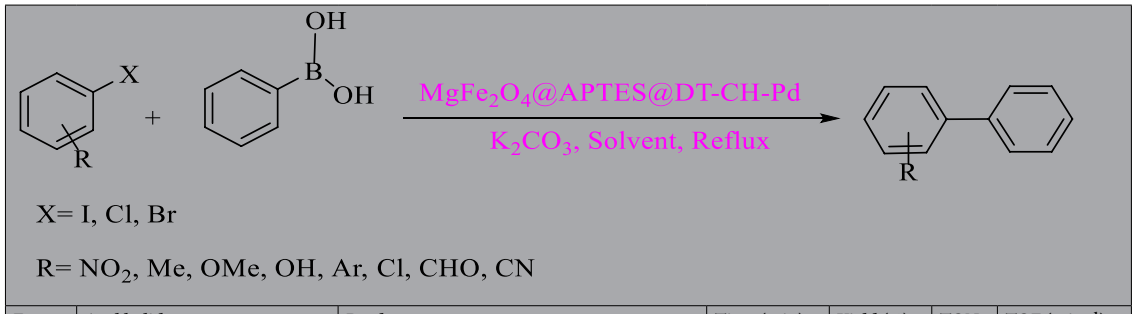

Entry	Aryl halide	Product	Time (min)	Yield (%)	TON	TOF (min^{-1})
12	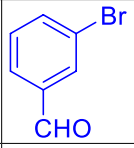	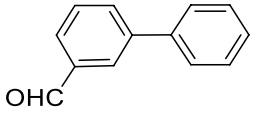	45	90	26.4	35.2
13	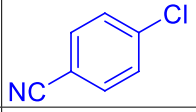	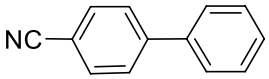	60	94	27.6	27.6
14	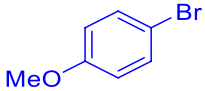	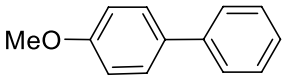	30	91	26.7	53.4

Table 2. Synthesis of carbon-carbon coupling reactions from Aryl halides utilizing $MgFe_2O_4$@APTES@DT-CH-Pd.

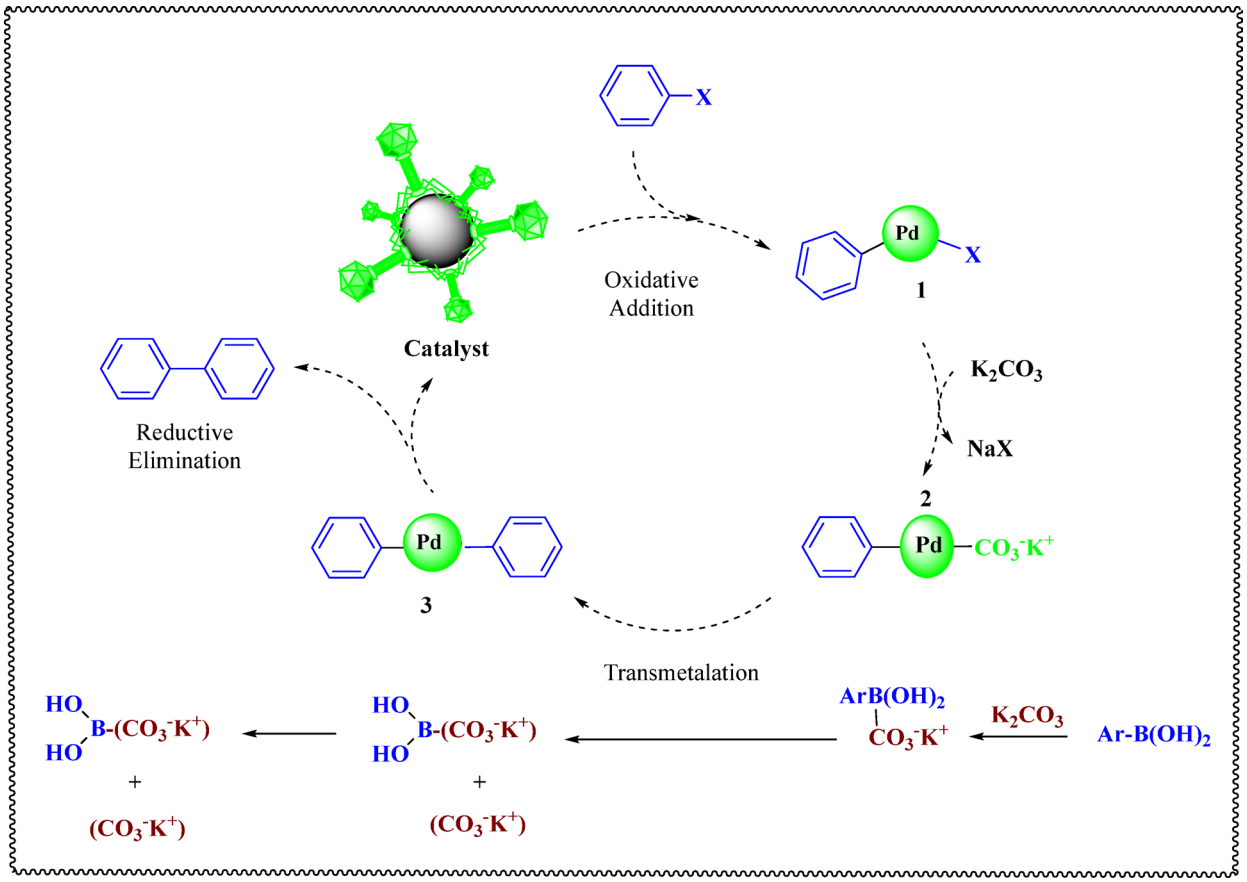

Fig. 10. Possible mechanism for Suzuki reaction.

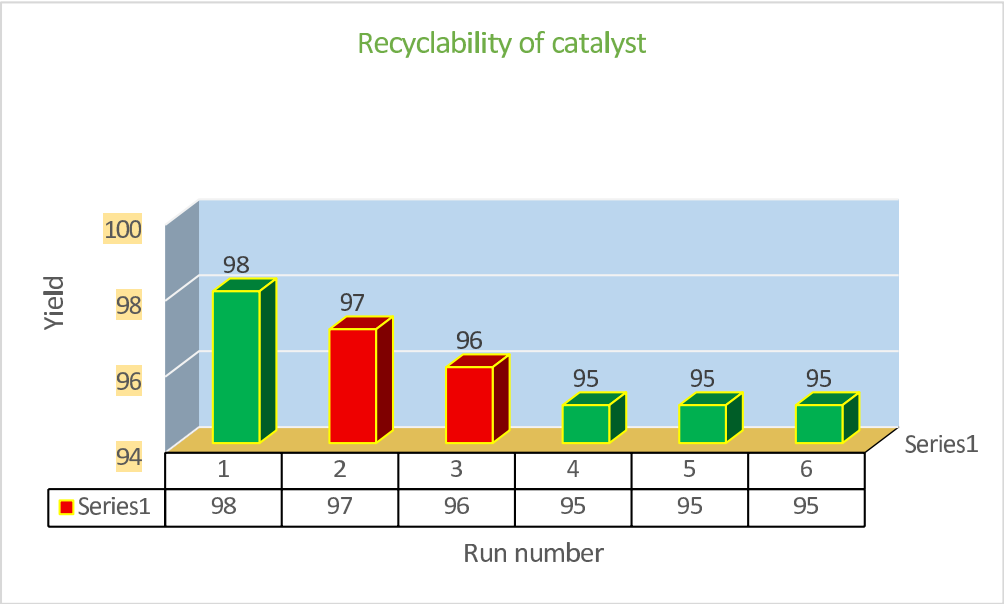

Fig. 11. Recyclability of $MgFe_2O_4$@APTES@DT-CH-Pd.

Entry	Catalyst	Ar-X	Product	Time (min)	Yield (%)	Ref.
1	MCM-Pd	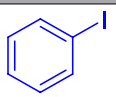	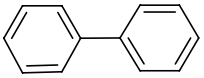	1440	74	[51]
2	MCM-41-VO	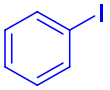	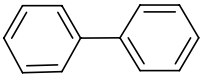	720	100	[52]
3	MCM@ACD-Pd	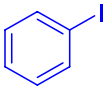	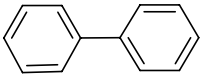	120	94	[53]
4	$MgFe_2O_4$@APTES@DT-CH-Pd	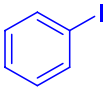	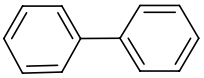	30 min	98	**This work**

Table 3. Comparison of the catalytic activity of $MgFe_2O_4$@APTES@DT-CH-Pd with previously documented methods in the Suzuki reaction.

biphenyl synthesis across six cycles without noticeable loss in its initial catalytic activity, as illustrated in Fig. 11. The initial decrease from 98% to 97%, then to 96%, and finally to 95%, suggests that the deactivation mechanisms are more active in the early cycles and then reach a more stable state. This may be due to the faster loss of the "more vulnerable active sites" in the first cycles, reaching an equilibrium between degradation and catalyst stability in the later cycles.

The efficiency of $MgFe_2O_4$@APTES@DT-CH-Pd as a nanocatalyst was evaluated by comparing its performance with that of other nanocatalysts reported in the literature, as summarized in Table 3. This comparison underscores its effectiveness in C-C coupling reactions relative to previously documented catalysts. Importantly, the nano-$MgFe_2O_4$@APTES@DT-CH-Pd exhibits significant advantages, such as reduced reaction times, excellent product yields, and the use of environmentally benign solvents. These results highlight its potential as a highly effective and versatile nanocatalyst for the synthesis of organic compounds.

Conclusion

The study introduces $MgFe_2O_4$@APTES@DT-CH-Pd, an innovative metallic nanocatalyst successfully developed, synthesized, and thoroughly characterized using cutting-edge methods such as FT-IR, TGA, EDS, SEM, XRD, ICP, and VSM. This catalyst demonstrated remarkable efficiency in facilitating C-C coupling reactions, delivering high yields within short timeframes. The functionalization of $MgFe_2O_4$ nanoparticles with DT-CH-Pd significantly boosted their catalytic activity and overall reaction performance. Furthermore, it exhibited excellent reusability by maintaining steady efficiency across multiple usage cycles. Importantly, the

$MgFe_2O_4$@APTES@DT-CH-Pd nano catalyst is easily synthesized from cheap and available materials and has several advantages, including easy separation, thermal stability in the reaction mixture, and reusability.

Data availability

All data generated or analyzed during this study are included in this published article and its supplementary information files.

Received: 8 August 2025; Accepted: 24 October 2025
Published online: 25 November 2025

References

1. Leal, E. et al. Effect of the surface treatment on the structural, morphological, magnetic and biological properties of MFe2O4 iron spinels (M = Cu, Ni, Co, Mn and Fe). *Appl. Surf. Sci.* **455**, 635–645. https://doi.org/10.1016/j.apsusc.2018.06.025 (2018).
2. Ahmadi, A., Sedaghat, T., Motamedi, H. & Azadi, R. Anchoring of Cu (II)-Schiff base complex on magnetic mesoporous silica nanoparticles: catalytic efficacy in one-pot synthesis of 5-substituted-1H-tetrazoles, antibacterial activity evaluation and immobilization of α-amylase. *Appl. Organomet. Chem.* **34**, e5572. https://doi.org/10.1002/aoc.5572 (2020).
3. Guo, Y. et al. Synthesis of magnetic core-shell carbon dot@MFe2O4 (M = Mn, Zn and Cu) hybrid materials and their catalytic properties. *J. Mater. Chem. A*. **4**, 4044–4055. https://doi.org/10.1039/c5ta10708c (2016).
4. Zhang, M. et al. Synthesis, characterization and catalytic behavior of MFe2O4 (M = Ni, Zn and Co) nanoparticles on the thermal decomposition of TKX-50. *J. Therm. Anal. Calorim.* **141**, 1413–1423. https://doi.org/10.1007/s10973-019-09102-x (2020).
5. Aschenaki, A. et al. Preparation of a magnetic and recyclable superparamagnetic silica support with a boronic acid group for immobilizing Pd catalysts and its applications in Suzuki reactions. *RSC Adv.* **11**, 33692–33702. https://doi.org/10.1039/d1ra04892a (2021).
6. Daneshafruz, H., Mohammadi, P., Barani, H. & Sheibani, H. Magnetic bentonite decorated with Pd nanoparticles and cross-linked Polyvinyl pyridine as an efficient nanocatalyst for Suzuki coupling and 4-Nitrophenol reduction reactions. *Sci. Rep.* **13**, 2001. https://doi.org/10.1038/s41598-023-27800-3 (2023).
7. Mirbagheri, R., Elhamifar, D. & Shaker, M. Yolk–shell structured magnetic mesoporous silica: a novel and highly efficient adsorbent for removal of methylene blue. *Sci. Rep.* **11**, 23259. https://doi.org/10.1038/s41598-021-02699-w (2021).
8. Foroughi, M. M. et al. Template-free synthesis of ZnO/Fe3O4/Carbon magnetic nanocomposite: nanotubes with hexagonal cross sections and their electrocatalytic property for simultaneous determination of oxymorphone and heroin. *Microchem J.* 170. https://doi.org/10.1016/j.microc.2021.106679 (2021).
9. Mirabella, F. et al. Ni-modified Fe3O4(001) surface as a simple model system for Understanding the oxygen evolution reaction. *Electrochim. Acta*. **389** https://doi.org/10.1016/j.electacta.2021.138638 (2021).
10. Meng, J. et al. A comparative study on effect of microwave sintering and conventional sintering on properties of Nd–Mg–Ni–Fe3O4 hydrogen storage alloy. *Int. J. Hydrogen Energy*. **35**, 8310–8316. https://doi.org/10.1016/j.ijhydene.2009.12.011 (2010).
11. Salokhe, A. et al. Magneto-structural and induction heating properties of MFe2O4 (M = Co, Mn, Zn) MNPs for magnetic particle hyperthermia application. *SN Appl. Sci.* **2** https://doi.org/10.1007/s42452-020-03865-x (2020).
12. Xue, J., Zhang, H., Zhao, J., Ou, X. & Ling, Y. Characterization and microwave absorption of spinel MFe2O4 (M = Mg, Mn, Zn) nanoparticles prepared by a facile oxidation-precipitation process. *J. Magn. Magn. Mater.* **514** https://doi.org/10.1016/j.jmmm.2020.167168 (2020).
13. Xu, Z. et al. Large-scale synthesis of Fe9S10/Fe3O4@C heterostructure as integrated trapping-catalyzing interlayer for highly efficient lithium-sulfur batteries. *Chem. Eng. J.* 422. https://doi.org/10.1016/j.cej.2021.130049 (2021).
14. Ranjith Kumar, E., Jayaprakash, R. & Kumar, S. The role of annealing temperature and bio template (egg white) on the structural, morphological and magnetic properties of manganese substituted MFe2O4 (M = Zn, Cu, Ni, Co) nanoparticles. *J. Magn. Magn. Mater.* **351**, 70–75. https://doi.org/10.1016/j.jmmm.2013.09.055 (2014).
15. Zhao, H. et al. In vitro toxicity evaluation of ultra-small MFe2O4 (M = Fe, Mn, Co) nanoparticles using A549 cells. *RSC Adv.* **5**, 68454–68460. https://doi.org/10.1039/c5ra11013k (2015).
16. Sun, F., Zeng, Q., Tian, W., Zhu, Y. & Jiang, W. Magnetic MFe2O4-Ag2O (M = Zn, Co, & Ni) composite photocatalysts and their application for dye wastewater treatment. *J. Environ. Chem. Eng.* **7** https://doi.org/10.1016/j.jece.2019.103011 (2019).
17. Bindu, K. & Nagaraja, H. S. Influence of cations in MFe2O4 (M: Fe, Zn, Ni, Sn) ferrite nanoparticles on the electrocatalytic activity for application in hydrogen peroxide sensor. *Mater. Res. Express*. **6** https://doi.org/10.1088/2053-1591/ab2ca8 (2019).
18. Zhang, M. et al. Catalytic effects of rGO-MFe2O4 (M = Ni, Co, and Zn) nanocomposites on the thermal decomposition performance and mechanism of energetic FOX-7. *J. Phys. Chem. A*. **124**, 1673–1681. https://doi.org/10.1021/acs.jpca.9b09711 (2020).
19. Al Yaqoob, K., Bououdina, M., Akhter, M. S., Al Najar, B. & Vijaya, J. J. Selectivity and efficient Pb and cd ions removal by magnetic MFe2O4 (M = Co, Ni, Cu and Zn)nanoparticles. *Mater. Chem. Phys.* **232**, 254–264. https://doi.org/10.1016/j.matchemphys.2019.04.077 (2019).
20. Garcia, S. M., Wong, A., Khan, S. & Sotomayor, M. D. P. T. A simple, sensitive and efficient electrochemical platform based on carbon paste electrode modified with Fe3O4@MIP and graphene oxide for folic acid determination in different matrices. *Talanta* 229. https://doi.org/10.1016/j.talanta.2021.122258 (2021).
21. Villa, S., Riani, P., Locardi, F. & Canepa, F. Functionalization of Fe3O4 NPs by silanization: use of amine (APTES) and thiol (MPTMS) silanes and their physical characterization. *Mater. (Basel)*. 9. https://doi.org/10.3390/ma9100826 (2016).
22. Hadrup, N. et al. Pulmonary toxicity of Fe2O3, ZnFe2O4, NiFe2O4 and NiZnFe4O8 nanomaterials: inflammation and DNA strand breaks. *Environ. Toxicol. Pharmacol.* **74**, 103303. https://doi.org/10.1016/j.etap.2019.103303 (2020).
23. Nawaz, Z. et al. Synthesis of new Pd(NHC)-PEPPSI type complexes as catalysts toward C-C cross-coupling reactions. *J. Mol. Struct.* **1243**, 130883. https://doi.org/10.1016/j.molstruc.2021.130883 (2021).
24. Panchal, U., Modi, K., Panchal, M., Mehta, V. & Jain, V. K. Catalytic activity of recyclable resorcinarene-protected antibacterial Pd nanoparticles in C-C coupling reactions. *Chin. J. Catal.* **37**, 250–257. https://doi.org/10.1016/S1872-2067(15)61021-X (2016).
25. Payamifar, S., Abdouss, M. & Poursattar Marjani, A. A review of using KCC-1-based heterogeneous nanocatalysts in the Suzuki reaction. *J. Organomet. Chem.* **1039**, 123795. https://doi.org/10.1016/j.jorganchem.2025.123795 (2025).
26. Geng, B. et al. High-efficiency PdNi single-atom alloy catalyst toward cross-coupling reaction. *Chin. Chem. Lett.* **35**, 108924. https://doi.org/10.1016/j.cclet.2023.108924 (2024).
27. Asadzadeh, F., Poursattar, A. & Marjani Improved one-pot synthesis of Suzuki-Miyaura coupling using a new heterogeneous nanocatalyst Ni anchored to the Fe3O4@MIL-101@-(CH2)3-Cl@Aa. *Inorg. Chem. Commun.* **181**, 115211. https://doi.org/10.1016/j.inoche.2025.115211 (2025).
28. Khandaka, H., Sharma, K. N. & Joshi, R. K. Aerobic Cu and amine free Sonogashira and Stille couplings of Aryl bromides/chlorides with a magnetically recoverable Fe3O4@SiO2 immobilized Pd(II)-thioether containing NHC. *Tetrahedron Lett.* **67**, 152844. https://doi.org/10.1016/j.tetlet.2021.152844 (2021).

29. Minami, A. et al. Enhancement of Elastin expression by transdermal administration of Sialidase isozyme Neu2. *Sci. Rep.* **11** https://doi.org/10.1038/s41598-021-82820-1 (2021).
30. Payamifar, S., Behrouzi, L., Poursattar, A. & Marjani The electrochemical coupling reactions of organic halides compound in a valuable and practical manner for CC and C–heteroatom formation: an overview. *Arab. J. Chem.* **17**, 105822. https://doi.org/10.1016/j.arabjc.2024.105822 (2024).
31. Baran, T., Akay, S. & Kayan, B. Fabrication of palladium nanoparticles supported on natural volcanic Tuff/Fe3O4 and its catalytic role in Microwave-Assisted Suzuki–Miyaura coupling reactions. *Catal. Lett.* **151**, 1102–1110. https://doi.org/10.1007/s10562-020-03378-7 (2021).
32. Supriya, S., Ananthnag, G. S., Shetti, V. S., Nagaraja, B. M. & Hegde, G. Cost-effective bio-derived mesoporous carbon nanoparticles-supported palladium catalyst for nitroarene reduction and Suzuki–Miyaura coupling by microwave approach. *Appl. Organomet. Chem.* **34** https://doi.org/10.1002/aoc.5384 (2020).
33. Beigiazaraghbelagh, P., Poursattar, A. & Marjani Carbon-based catalysts: advances in synthesizing N-heterocyclic compounds using graphene family and graphite oxide. *Res. Chem. Intermed.* **50**, 485–531. https://doi.org/10.1007/s11164-023-05205-1 (2024).
34. Li, J., Yang, S., Wu, W. & Jiang, H. Recent advances in Pd-Catalyzed Cross-Coupling reaction in ionic liquids. *Eur. J. Org. Chem.* **2018**, 1284–1306. https://doi.org/10.1002/ejoc.201701509 (2018).
35. Han, C. et al. Enhanced support effects in single-atom copper-incorporated carbon nitride for photocatalytic Suzuki cross-coupling reactions. *Appl. Catal. B Environ.* **320**, 121954. https://doi.org/10.1016/j.apcatb.2022.121954 (2023).
36. Aabaka, S. R. et al. Nanocellulose supported PdNPs as in situ formed nano catalyst for the Suzuki coupling reaction in aqueous media: A green approach and waste to wealth. *J. Organomet. Chem.* **937**, 121719. https://doi.org/10.1016/j.jorganchem.2021.121719 (2021).
37. Wang, C. et al. Photothermal Suzuki coupling over a metal halide Perovskite/Pd nanocube composite catalyst. *ACS Appl. Mater. Interfaces*. **14**, 17185–17194. https://doi.org/10.1021/acsami.1c24710 (2022).
38. Zhang, Y. et al. Porous, Tremella-like NiFe2O4 with ultrathin nanosheets for ppb-Level toluene detection. *Crystals* 13. https://doi.org/10.3390/cryst13060865 (2023).
39. Dighe, S. U., Juliá, F., Luridiana, A., Douglas, J. J. & Leonori, D. A photochemical dehydrogenative strategy for aniline synthesis. *Nature* **584**, 75–81. https://doi.org/10.1038/s41586-020-2539-7 (2020).
40. Gu, Q., Jia, Q., Long, J. & Gao, Z. Heterogeneous photocatalyzed C–C Cross-coupling reactions under Visible-light and Near-infrared light Irradiation. *chemcatchem.* **11** 669. (2019).
41. Takita, S., Suzuki, H., Tomiyasu, K., Kamazawa, K. & Watanabe, T. Ultrasound velocity measurements in the geometrically-frustrated spinel ZnFe2O4. *J. Phys. Conf. Ser.* https://doi.org/10.1088/1742-6596/592/1/012108 (2014).
42. Rangraz, Y., Nemati, F. & Elhampour, A. A novel magnetically recoverable palladium nanocatalyst containing organoselenium ligand for the synthesis of biaryls via Suzuki-Miyaura coupling reaction. *J. Phys. Chem. Solids.* **138**, 109251. https://doi.org/10.1016/j.jpcs.2019.109251 (2020).
43. Scattolin, T. et al. Synthesis of novel allyl palladium complexes bearing purine based NHC and a water soluble phosphine and their catalytic activity in the Suzuki-Miyaura coupling in water. *Appl. Organomet. Chem.* **32**, e4034. https://doi.org/10.1002/aoc.4034 (2018).
44. Bangale, S. 57 bioinfo publications microbial gas sensing property of Bacillus subtilis with mixed metal catalyst MGFE2O4. *Int. J. Microbiol. Res.* **3**, 975–5276 (2011).
45. Gong, T. & Tang, Y. Preparation of multifunctional nanocomposites Fe3O4@SiO2-EDTA and its adsorption of heavy metal ions in water solution. *Water Sci. Technol.* **81** https://doi.org/10.2166/wst.2020.099 (2020).
46. Huang, X. et al. Studies on Re-188 labeling and in vivo distribution of magnetic nanoparticles with different morphologies and sizes. *J. Inorg. Organomet. Polym. Mater.* **34** https://doi.org/10.1007/s10904-023-02830-6 (2023).
47. Nasaj, M. et al. Vancomycin and nisin-modifed magnetic Fe3O4@SiO2 nanostructures coated with Chitosan to enhance antibacterial efciency against methicillin resistant Staphylococcus aureus (MRSA) infection in a murine superfcial wound model. *BMC Chem.* **18** https://doi.org/10.1186/s13065-024-01129-y (2024).
48. Zhang, L. et al. Control synthesis of magnetic Fe3O4–chitosan nanoparticles under UV irradiation in aqueous system. *Curr. Appl. Phys.* **10**, 828–833. https://doi.org/10.1016/j.cap.2009.10.002 (2010).
49. Zia, J., Rafi, M., Aazam, E. & Riaz, U. Microwave—assisted catalytic degradation efficiency of non-steroidal anti-inflammatory drug (NSAIDs) using magnetically separable magnesium ferrite (MgFe2O4) nanoparticles, clean technol. *Environ. Policy*. **27**, 83–96. https://doi.org/10.1007/s10098-024-02835-w (2024).
50. Desai, H., Kumar, A. & Tanna, A. Structural and magnetic properties of MgFe2O4 ferrite nanoparticles synthesis through auto combustion technique. *Eur. Chem. Bull. Eur. Chem.* 186–190. https://doi.org/10.17628/ecb.2021.10.186-190 (2021).
51. Das, T., Uyama, H. & Nandi, M. Pronounced effect of pore dimension of silica support on Pd-catalyzed Suzuki coupling reaction under ambient conditions. *New. J. Chem.* **42**, 6416–6426. https://doi.org/10.1039/c8nj00254a (2018).
52. Karimi, B., Barzegar, H. & Vali, H. Au–Pd bimetallic nanoparticles supported on a high nitrogen-rich ordered mesoporous carbon as an efficient catalyst for room temperature Ullmann coupling of Aryl chlorides in aqueous media. *Chem. Commun.* **54**, 7155–7158. https://doi.org/10.1039/C8CC00475G (2018).
53. Amini, M. M., Mohammadkhani, A. & Bazgir, A. Dicarboxylic Acid-Functionalized MCM-41 with embedded palladium nanoparticles as an efficient heterogeneous catalyst for C–C coupling reactions. *ChemistrySelect* **3**, 1439–1444. https://doi.org/10.1002/slct.201702622 (2018).

Author contributions

Magda H. Abdellattif . Mohammad Abu Shuheil. Munthar Kadhim Abosaoda. Rekha M M. Rasha Eldalawy. Subhashree Ray. Kattela Chennakesavulu. and Renu Sharma. Funding acquisition, Supervision, Validation, Investigation, Methodology, Conceptualization, Resources, Writing-review & editing.

Funding

No funding available.

Declarations

Competing interests

The authors declare no competing interests.

Declaration of competing interest

The authors declare that they have no known competing financial interests or personal relationships that could have appeared to influence the work reported in this paper.

Additional information

Supplementary Information The online version contains supplementary material available at https://doi.org/10.1038/s41598-025-25753-3.

Correspondence and requests for materials should be addressed to M.A.l.H. or M.A.S.

Reprints and permissions information is available at www.nature.com/reprints.

Publisher's note Springer Nature remains neutral with regard to jurisdictional claims in published maps and institutional affiliations.